MONAGHAN, B.J., NIGHTINGALE, S.A., CHEN, L., and BROOKS, G.A. The dissolution behaviour of selected oxides in $CaO-SiO_2-Al_2O_3$ slags. *VII International Conference on Molten Slags Fluxes and Salts*, The South African Institute of Mining and Metallurgy, 2004.

The dissolution behaviour of selected oxides in $CaO-SiO_2-Al_2O_3$ slags

B.J. MONAGHAN*, S.A. NIGHTINGALE*, L. CHEN*, and G.A. BROOKS†
**University of Wollongong, Materials Engineering and Institute of Steel Processing and Products, Wollongong, Australia*
†McMaster University, Department of Materials Science and Engineering, Hamilton, Ontario, Canada

The dissolution of alumina and magnesia has been investigated using laser scanning confocal microscopy (alumina) and a rotating finger apparatus (magnesia) to assess the effects of temperature, composition and forced convection on the rate of dissolution in $CaO-SiO_2-Al_2O_3$ based slags. The two techniques have differing strengths and limitations, and provide complementary methods for studying dissolution.

Alumina dissolution was studied for temperatures from 1477 to 1577°C. Based upon the data, the rate controlling mechanism was thought to be mass transfer control in the slag. The diffusion coefficients for the alumina particles are estimated to be in the range 10^{-11} to 10^{-10} $m^2.s$.

MgO degradation for sample rotation speeds of 50 to 800 rpm at 1500 and 1530°C was studied for both congruent and incongruent dissolution. The results show that the rate of dissolution for this is primarily controlled by a diffusion mass transfer mechanism for congruent dissolution except at the highest rotation speed. For incongruent dissolution, the mechanism is much more complex, with the morphology and distribution of the spinel reaction product having a significant effect. At high speeds and prolonged times, mechanical forces played a major role in the degradation process.

Keywords; kinetics, corrosion, refractories, dissolution rate, inclusions, mass transfer, slags, steelmaking

Introduction

Dissolution of refractories and inclusions in slags has been traditionally measured using dip techniques whereby a refractory material is dipped in a molten slag and held for a period of time, removed, then analysed for slag penetration and/or corrosion. The dipped refractory sample may be static or rotated, as is the case in the classic rotating finger or disk method. These methods have been used to generate much of much of the data that is in the literature[2–9]. The dip technique is a robust and simple method for generating kinetic data in what is a testing environment; it is particularly suited to the rotating methods where there is some capability of selecting the dissolution rate-controlling mechanism that is being studied. While these techniques have elucidated the mechanism of dissolution of many refractory slag systems, there has always been some doubt the data generated represented the dissolution behaviour of micro-particles (inclusions) in slags.

Recently a new technique, the high temperature laser scanning confocal microscope (LSCM)10–13, has become available that offers possibilities for analysing the dissolution behaviour of micro-particles in a slag directly (see confocal experimental details below for a description of the technique). Sridhar and co-workers10–12 have demonstrated that dissolution measurements of inclusions in the bulk of a slag can be made in the LSCM, providing the slag is transparent to the interrogation laser used in the instrument. This precludes the use of important slag systems that include transition metal oxides such as FeO, but offers numerous possibilities to test whether the dissolution behaviour of micro-particles in a slag system is significantly different from 'macro' refractory dissolution.

Most 'macro' dissolution studies have shown that alumina dissolution in CaO-SiO2-Al2O3 is mass transfer controlled2–9,14. This has been confirmed by LSCM measurements10–12 and another micro-particle study. What is not clear yet is whether the mass transfer and diffusion coefficients generated by the two different techniques are consistent. The reason for the uncertainty is at least in part due to the fact that LSCM slag dissolution measurements are in their infancy and many of the observed phenomena are novel. While the LSCM is opening up new avenues for fundamental research into dissolution and other phenomena, it will not be able to answer many of the important questions on dissolution that are asked of a ceramic or refractory material. To obtain an understanding of the dissolution behaviour over the spectrum of materials that dissolve in slags, full use of all available experimental techniques is required.

Ideally a complementary study should be carried out on as near identical solid oxide-slag system as possible by both the LSCM and the rotating finger technique. The authors plan to carry out such a study in the near future. What is presented here are two separate dissolution studies. One investigates the dissolution behaviour of micro-particles in a $CaO-SiO_2-Al_2O_3$ slag using the LSCM, the other studies the dissolution of direct bonded MgO in $CaO-SiO_2-Al_2O_3-MgO-FeO_x$.

Dissolution behaviour of alumina micro-particles in a $CaO\text{-}SiO_2\text{-}Al_2O_3$ slag using the LSCM

Confocal experimental details

A series of experiments was carried out in a high temperature laser scanning confocal microscope (LSCM) to assess the rate and mechanism of dissolution of alumina micro-particles (inclusions) in $CaO\text{-}SiO_2\text{-}Al_2O_3$. In an LSCM, high resolution images of a material can be obtained that would be impossible by most other conventional imaging techniques. Such imaging enables real time *in situ* observations of high temperature transient phenomena. Details of the technique have been widely published[10,13]. What follows is a general outline of the technique used in this study.

A schematic of the laser-lens set-up and pinhole used in an LSCM is given in Figure 1. In an LSCM, laser light is focused by an objective lens onto the sample and the sample reflected light is focused onto a photo detector via a beam splitter. An image is built up by scanning the focused spot relative to the sample. This is then stored in an imaging system for subsequent display. Through the use of a confocal pinhole, only light incident from the focal plane is permitted to pass through to the photo detector. Hence, an extremely thin optical section is created, providing a high resolution image. Magnifications of up to 1350 times can be achieved and in theory sub-micron sample features can be resolved, though in the author's experience, approximately 1 mm is the resolution limit. The laser used in the microscope is an He-Ne laser with a wavelength of 632.8 nm and a beam diameter of 0.5 μm.

The experiments consisted of addition of a few alumina particles to a pre-fused slag. Rapid heating of the slag and alumina particles in air to the desired temperature was performed using an infrared furnace. The system was held at temperature until the alumina particle completely dissolved in the slag. The slag, the alumina particle, the temperature and time were logged and recorded to video throughout the experiment. After each experiment the video recordings were analysed to obtain the change in particle area with time. The analysis procedure involves capturing and digitizing image stills from the video, then reading the digitized image into the Scan Image image analysis software. Once in the digital analysis system, a border is manually drawn around the alumina particle. This drawn object is then converted to an area. On the assumption that the particle is a sphere, a radius is then calculated from the area. It is this calculated radius that forms the basis of the results presented in this paper. An example of images

Figure 2. A typical example of an image obtained from the LSCM showing an alumina particle in a $CaO\text{-}SiO_2\text{-}Al_2O_3$ slag

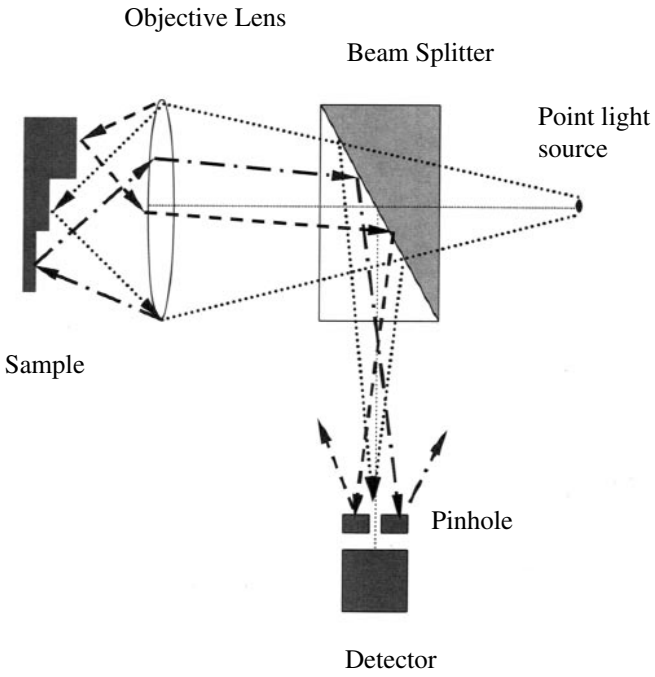

Figure 1. A schematic showing the confocal lens set-up and pinhole

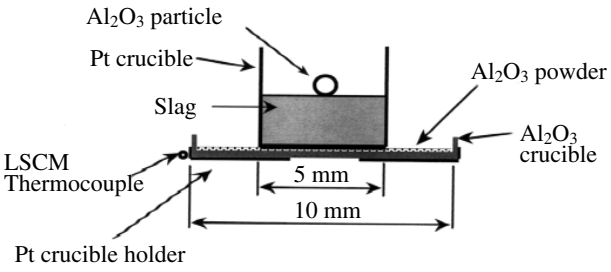

Figure 3. A schematic of the sample and crucible configuration in the LSCM furnace

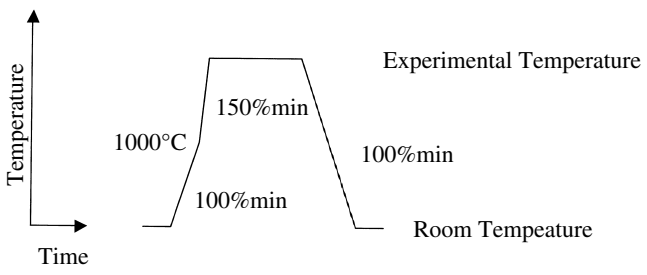

Figure 4. A schematic of the temperature programme used in the LSCM experiments

obtained from this technique is given in Figure 2.

The crucible configuration and temperature profile used in the experiments are given in Figures 3 and 4. Experiments were carried out over the temperature range of 1477 to 1577°C.

A B type thermocouple is used for temperature measurement. In Figure 3 it can be seen that the thermocouple is remote from the sample. To ensure an accurate temperature measurement, a temperature calibration is carried out whereby a type S thermocouple is welded to the side of the platinum crucible containing slag material. This crucible, slag and type S thermocouple are placed in the LSCM and heated through the experimental temperature range. The difference in the LSCM and calibration thermocouple measurement is logged and is used to correct the temperatures in subsequent experiments.

The compositions of the alumina and slags used in this study are given in Table I. The reported compositions are of ICP measurements on slag after preparation. The slags were prepared by pre-melting appropriate mixtures of $CaCO_3$, SiO_2 and Al_2O_3, quenching the fused slag in water and then crushing the resultant glass. This process was repeated to obtain a homogenous slag. The crushed slag was then melted *in situ* in the LSCM prior to running an experiment. Slag compositions were chosen to ensure that the slag was transparent to the laser imaging system. Under such conditions it is possible to observe the alumina particle subsurface in the bulk of the slag. The alumina particles were sieved prior to use to obtain particles around 100 μm in diameter.

Table I
Composition of materials used in this study

Mass%	CaO	SiO_2	Al_2O_3	Other
Slag 1	16.3	64.5	19.3	-
Slag 2	28.0	48.3	23.7	-
Alumina particle	0.08	-	98.6	0.6

Results/discussion of the LSCM dissolution experiments

The results of the alumina dissolution experiments are given in Figures 5 and 6 where R represents the radius of the particle at time t and R_O is the radius of the particle at time zero. Time zero is defined as the point at which the measured temperature reached the set experimental temperature. It is likely that for all but the highest temperature experiments in each slag system this is a reasonable assumption, though as yet the authors have made little attempt to quantify the error associated with this assumption. In Figures 5 and 6 it can be seen that increasing temperature increases the rate of dissolution of the alumina and also that the rate of alumina dissolution is greater in Slag 2.

The effect of temperature is best explained by considering the effect of temperature on the likely rate controlling mechanisms of mass transport control in the slag phase or chemical reaction control at the particle slag interface.[16]

For a first order chemical reaction the following rate equation for dissolution can be written

$$J = kC_A \qquad [1]$$

where J is the molar flux of A per unit area, k is a rate constant, and C_A is the molar concentration of A.

For a mass transport controlled process, Fick's law can be applied to diffusion across the boundary layer; therefore we can write

$$J = D\frac{\Delta C}{\delta} \qquad [2]$$

where J is the molar flux as before, D is the diffusion coefficient, and ΔC is the concentration gradient across the boundary layer, δ.

It is known both D and k show Arrhenius behaviour with temperature. For a property Y that shows Arrhenius behaviour, the following relation holds

$$Y = Y_o e^{-A/(RT)} \qquad [3]$$

where Y_0 is a pre-exponential constant, A is an activation energy, R is the gas constant, and T is temperature. Properties that show Arrhenius behaviour increase with increasing temperature. Therefore increasing temperature would increase k or D and thereby increase J, the dissolution rate.

It is less clear why changing the slag composition affects the rate of dissolution. The explanation of why and how changing the slag composition changes the rate of dissolution will be dependent on which mechanism was rate controlling.

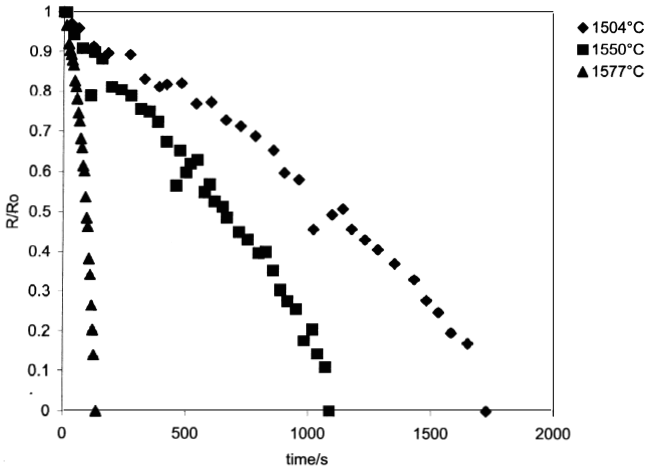

Figure 5. A plot of (R/R_O) versus time at different temperatures for an alumina particle in Slag 1

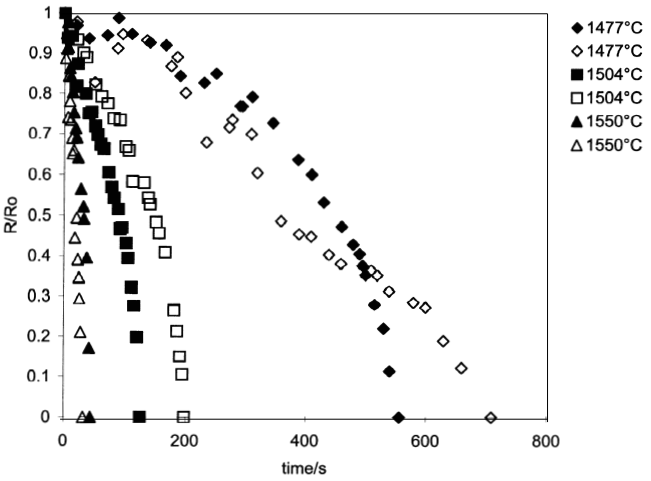

Figure 6. A plot of (R/R_O) versus time at different temperatures for an alumina particle in Slag 2

Establishing the rate controlling mechanism

The alumina dissolution reaction can be represented in simple terms by

$$Al_2O_3(s)\Delta\left(Al_2O_3\right) \quad [4]$$

where the brackets '( )' signify in solution in the slag. The dissolution kinetics of a micro-particle in a fluid are described well by the shrinkage core model[16]. Using this model it can be shown that, for chemical reaction control and mass transfer control in the slag, phase in the stokes regime can be represented by Equations [5] and [6].

$$\left(\frac{R}{R_O}\right)-1=\frac{bkC_{Al_2O_3bulk}}{R_O\rho_{particle}}t \quad [5]$$

$$\left(\frac{R}{R_O}\right)^2-1=\frac{b2D\left(C_{Al_2O_3\ bulk}-C_{Al_2O_3\ sat.}\right)}{R_O^2\rho_{particle}}t \quad [6]$$

where R is the radius, R_O is the radius at time zero, k is a chemical reaction rate constant, D is the diffusion coefficient of alumina in the slag, $\rho_{particle}$ is the density of the dissolving particle, t is time, b is the stoichiometric coefficient of Equation [1], and C is the molar concentration in the slag phase. The subscript *sat.* is for saturation and represents the interfacial concentration at the particle boundary layer interface. Details of the derivations of Equations [5] and [6] are given in Levenspiel[16].

From Equations [5] and [6] it can be seen that plots of $\left(\frac{R}{Ro}\right)$-1 versus time for chemical reaction control or $\left(\frac{R}{Ro}\right)^2$-1 versus time for mass transfer control should be linear and pass through the origin if the respective method is rate controlling. The rate data are re-plotted in Figures 7 and 8 for Slags 1 and 2 respectively, to test for linearity with time for the rate controlling mechanisms. Figures 7a and 8a show the data re-plotted assuming chemical reaction control. Figures 7b and 8b show the data re-plotted assuming mass transport control. The data shown in these Figures have also been linearly regressed, the fits shown by solid lines on the graphs. The equations and degree of fit parameter (R^2) representing these regression lines are also shown. Inspection of Figures 7 and 8 show that within the scatter in the data either mechanism could be argued to be rate controlling.

The degree of fit parameter (R^2) for both the 'a' and 'b' plots are mostly greater that 0.9. This is an indication that the plots are reasonably linear with time. In general, the degree of fit parameter (R^2) tends to be slightly higher for mass transfer control but given the scatter in the data, this cannot be taken as conclusive evidence for said mechanism. The principle conclusion that may be drawn from these plots is that given the scatter in the data, the plots shown in Figures 7 and 8 are not suitable for discriminating between the different controlling mechanisms.

If mass transfer in the slag phase were rate controlling then it would be reasonable to expect that altering the

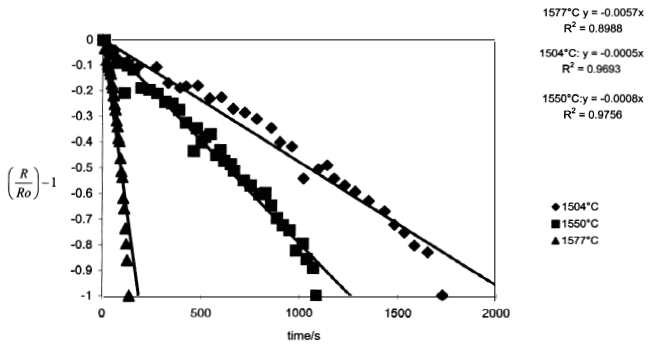

Figure 7a. A plot of $\left(\frac{R}{RO}\right)$ -1 versus time at different temperatures for an alumina particle in Slag 1. The solid lines and equations represent linear regression fits to the data

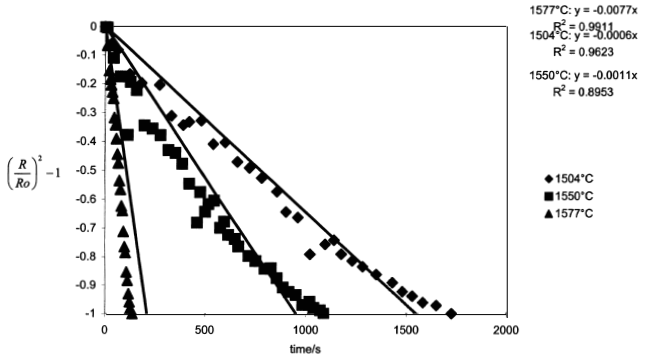

Figure 7b. A plot of $\left(\frac{R}{RO}\right)^2$-1versus time at different temperatures for an alumina particle in Slag 1. The solid lines and equations represent linear regression fits to the data

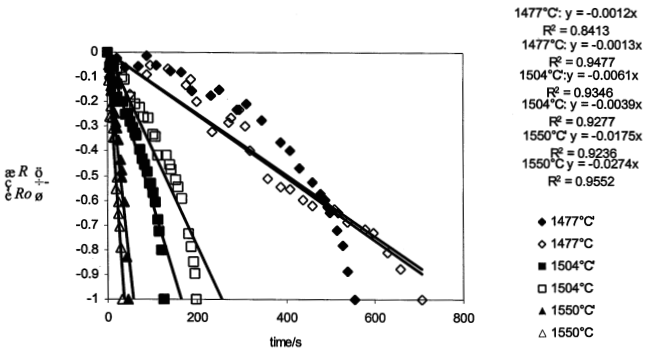

Figure 8a. A plot of $\left(\frac{R}{RO}\right)$-1 versus time at different temperatures for an alumina particle in Slag 2. The solid lines and equations represent linear regression fits to the data

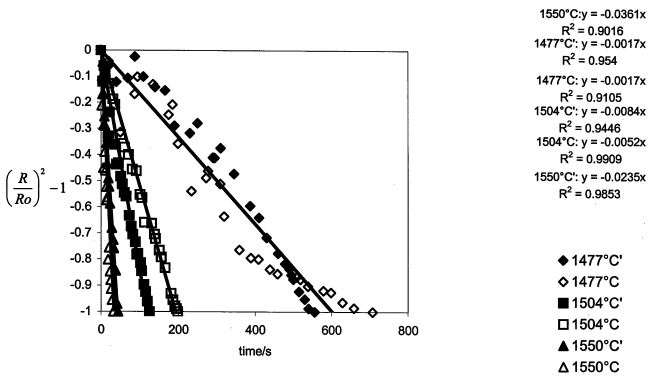

Figure 8b. A plot of $\left(\frac{R}{RO}\right)^2$-1versus time at different temperatures for an alumina particle in Slag 2. The solid lines and equations represent linear regression fits to the data

composition of the slag in such a way that the viscosity changed significantly, would cause a significant change in the dissolution rate. Lowering the viscosity would decrease δ, the boundary layer thickness, thereby increasing the dissolution rate[16,17]. Also lowering the viscosity would increase the diffusivity and again increase the dissolution rate, as demonstrated by the Eyring[17] relation in Equation [7]

$$D = \frac{k_b T}{\eta \lambda} \qquad [7]$$

where k_b is the Boltzman constant, T is temperature, η is viscosity, and λ is the jump frequency.

The slopes, m, generated from the regression analysis of the data for mass transport control given in Figures 7b and 8b can be used to obtained diffusion coefficients by solving Equation [8].

$$m = \frac{b2D\left(C_{Al_2O_3 bulk} - C_{Al_2O_3 sat.}\right)}{R_O^2 \rho_{particle}} \qquad [8]$$

The stoichiometric coefficient, b, for the alumina dissolution reaction as written in Equation [1] is 1. Molar concentrations are given in Table II. Saturation values were calculated using MTDATA thermodynamic software[18]. Slag density values were calculated using Slags Model[19]. The density of the alumina particle at a given temperature is listed in Table III. The particle density was measured at 20°C using the pycnometer method and corrected for expansion at higher temperatures using standard reference data[20]. The R_O, the slopes from Figures 7b and 8b, and the diffusion coefficients calculated from evaluating Equation [8] are given in Table IV.

Table II
Composition and property data for diffusion calculation

	Slag	T/°C	Al_2O_3 Mass %	Density kg.m^{-3}	CAl_2O_3 mole.m^{-3}	ΔC mole.m^{-3}
At saturation	1	1504	26.3	2541	6545	-1815.13
At saturation	1	1550	29.8	2550	7440	-2731.83
Aat saturation	1	1577	32.3	2558	8089	-3393.44
At saturation	2	1477	24.9	2636	6428	-599.80
At saturation	2	1504	27.9	2635	7218	-1409.78
At saturation	2	1550	34.3	2654	8923	-3141.12
Slag bulk	1	1504	19.3	2500	4730	-
Slag bulk	1	1550	19.3	2488	4708	-
Slag bulk	1	1577	19.3	2482	4696	-
Slag bulk	2	1477	23.7	2508	5828	-
Slag bulk	2	1504	23.7	2500	5809	-
Slag bulk	2	1550	23.7	2488	5782	-

Table III
Alumina particle density

T/C	kg.m^{-3}	mole.m^{-3}
20*	3720	36471
1504	3574	35038
1550	3569	34986
1577	3565	34956
1477	3577	35068
1477	3577	35068
1504	3574	35038
1504	3574	35038
1550	3569	34986
1550	3569	34986

*The density was measured at 20°C using the pycnometer method and corrected for expansion at higher temperatures using standard reference data[20]

The diffusion coefficients in Table IV are in reasonable agreement with other reported diffusion coefficients in $CaO\text{-}SiO_2\text{-}Al_2O_3$[9,14]. Cooper and Kingery[9] reported effective diffusion coefficients of between 9.1 x 10^{-12} to 33 x 10^{-11} m^2.s^{-1} over the temperature range of 1480 to 1550°C for sapphire in liquid $CaO\text{-}SiO_2\text{-}Al_2O_3$. Choi *et al.*[14] reported diffusivity values of between 1 x 10^{-10} and 3 x 10^{-10} m^2.s^{-1} over the temperature range used in this investigation. The Choi *et al.*[14] data are quoting Henderson *et al.*[21] diffusion coefficients. (At the time of writing this article, the original source was not available to the authors.) While there is significant uncertainty over the diffusion coefficients calculated from this study, principally due to the uncertainty in R_O, the fact that they are in broad agreement with other reported data is encouraging and gives credence to the experimental approach used.

The effect of viscosity on the diffusion coefficient is shown in Figure 9. The viscosity was calculated using the Riboud model[22]. It can be seen that for a given temperature, decreasing the viscosity of the slag increases the diffusion coefficient. This is in keeping with what is predicted for mass transport control for alumina diffusion and is a strong indicator that mass transfer is the controlling mechanism in this study.

Sources of error in the data

LSCM measurement of dissolution rates is a relatively new

Table IV
Calculated diffusion coefficients

Slag	R_O/microns	T/°C	Slope	Diffusion coefficients m^{2}s^{-1}
1	57.3	1504	-0.0006	1.90E-11
1	45.6	1550	-0.0011	1.46E-11
1	52.7	1577	-0.0077	1.10E-10
2	44.8	1477	-0.0017	9.98E-11
2	55.0	1477	-0.0017	1.50E-10
2	50.1	1504	-0.0052	1.62E-10
2	54.4	1504	-0.0084	3.09E-10
2	35.0	1550	-0.0235	1.60E-10
2	30.5	1550	-0.0361	1.87E-10

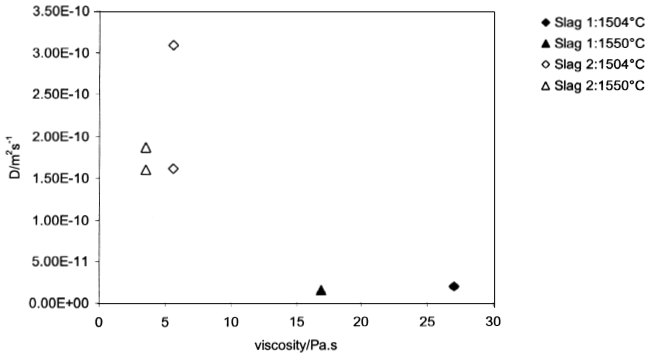

Figure 9. Effect of slag viscosity on the calculated diffusion coefficient

field with much of the ground-breaking research being carried out by Sridhar, Cramb and their co-workers[10–12]. There is much work to be carried out to assess the limitations of the applicability of the shrinkage core model to the experimental data; evaluation of R_O; effect of particle rotation and rotation rate on the dissolution rate; errors involved in use of non-spherical particles but carrying out a spherical analysis; difficulties in analysing composition gradients within the particle; and Stokes law limitations on the rate of particle sinking into the slag. Regardless of these limitations, this work and work by other researchers[10–12] demonstrates that the LSCM will be an important tool in evaluating and elucidating the dissolution behaviour of micro-particles in slags.

Dissolution of MgO in slag with forced convection

Refractory materials based on magnesium oxide (MgO) are widely used to contain the molten metal, slag and hot gases in steel processing vessels. Studies of MgO immersed in molten slags under static conditions have found that a dense spinel ($MgO.Al_2O_3$) or magnesiowustite ((Mg,Fe)O) layer may form at the MgO surface, protecting the MgO from further degradation.[23–27] The formation of these layers involves the counter-diffusion of ions, and is controlled by mass transfer. Layer thickness depends on the relative rates of formation of the solid solution (ss) at the MgO/ss interface, and the dissolution of the ss at the ss/liquid interface.

Goto *et al.*[28] performed cup tests on MgO/MgO-Al_2O_3 spinel refractories using a CaO-SiO_2-Al_2O_3 slag. They found that the spinel grain was subject to congruent dissolution, but the MgO dissolved incongruently, resulting in the formation of secondary spinel a short distance away from the refractory-slag interface. They postulated that this occurred because there was insufficient concentration of Al_2O_3 at the interface due to localized enrichment with MgO. More recent studies of MgO dissolution have also reported that the solid solution layer either formed at a distance from the solid surface, or initially formed there and then became detached and moved out into the liquid slag.[29,30] Under these conditions, this layer could be easily removed by forced liquid flow.

Studies of dissolution under dynamic conditions have focused on alumina based materials in contact with a variety of slag types. For forced convection flow it has been reported that the direct dissolution of alumina was controlled by mass transport across a boundary layer, as indicated by the dissolution rate being related to the square root of angular velocity.[9,31] Indirect dissolution of single crystal alumina in CaO-MgO-Al_2O_3-SiO_2 melts has been studied by Sandhage and Yurek.[2–4] Spinel was formed at 1450 and 1550°C, with varying slag compositions and rotation speeds of 100 to 1400 rpm. With slag containing 10% MgO, the spinel layer was attached to the alumina only at infrequent points, with slag trapped between the sapphire and the spinel. At higher MgO contents, a complete spinel layer was formed at the interface remained at a constant thickness over time. They concluded that even with forced convection flow, a steady state was quickly reached where the rate of spinel formation was equal to its rate of dissolution in the melt. Solid state diffusion through the solid spinel layer and liquid phase diffusion through the boundary layers were the rate controlling processes.

However, similar studies of the dissolution of MgO refractories in slag have not been reported.

Experimental method

A series of experiments was developed to study the effect of slag composition, temperature and liquid flow on the dissolution of MgO in steelmaking slags under highly controlled conditions. Of particular interest were the effects of alumina in the dissolution process, and the effects on the overall rate of degradation of forced convection flows.

A matrix of experiments was devised totalling thirty-one distinct experimental conditions. The conditions of each experiment are summarized in Table V.

A molybdenum disilicide vertical tube furnace with water-cooled end caps was used for all experiments. The hot zone in the furnace was approximately 50 mm long with a temperature variation of ±2°C at 1500°C. Two slag compositions were used: one without Al_2O_3 and one with 20% Al_2O_3. Two temperatures were used: 1500°C and 1530°C. Compressed air (industrial grade) from a bottle was regulated through a flow rotameter, passing through a dehumidifying vessel before entering the bottom of the furnace. The flow rate maintained for all experiments was 150 ml/min.

The cylindrical MgO test samples* (20 mm OD and 25 mm in length) were of high purity MgO (>97%), and had a

Table V
Experimental Conditions

Slag 1—No Al_2O_3 46% SiO_2 46% CaO 5% FeO_x 3% MgO						Slag 2–20% Al_2O_3 36% SiO_2 36% CaO 20% Al_2O_3 5% FeO_x 3% MgO					
T= 1530°C											
Speed (rpm)	15 min	30 min	45 min	60 min	90 min	Speed (rpm)	15 min	30 min	45 min	60 min	90 min
50	•					50	•				
200	•					200	•				
400	•					400	•				
600	•					600	•				
800	•	•	•	•	•	800	•	•	•	•	•
T=1500°C											
Speed (rpm)						Speed (rpm)					
600	•					600	•				
800	•		•		•	800	•	•		•	•

• Indicates experiments carried out in this study

density of greater than 96% theoretical. The MgO samples (20 mm O.D) were rotated by a variable speed motor aligned above the furnace

Chemical analyses of the slags recovered from the experiments were carried out by using X-ray fluorescence techniques. Standard ceramographic methods were used to prepare samples for microcopy.

Results

As rotation speed increased there was a change in the profile of the corroded samples. At lower speeds, most of the dissolution occurred at the slag/refractory/air interface. At higher speeds there was also some rounding of the bottom corners of the samples. Prolonging time at 800 rpm had an even greater effect, with loss from the bottom of the samples increasing greatly as time increased so that samples tested for 60 and 90 min became cone shaped, as illustrated in Figure 10.

Table VI shows the bulk MgO concentrations measured for each slag after a certain time for a given slag composition and sample rotation speed. Figure 11 shows how the MgO content in the slag varied after 15 minutes as a function of rotation speed for both slags A and B at 1530°C. Figure 3 gives MgO content in the slag as a function of time for a rotation speed of 800 rpm for both slags at two temperatures.

Both slags had a lime:silica ratio of 1 and a starting MgO content of 3.0 wt%. Calculations from phase diagrams indicate that Slag 1 will have a saturation MgO content of 19.1% at 1530°C and 18.5% at 1500°C, and that Slag 2 will have a saturation MgO content of 19.0% at 1530°C and 18.4% at 1500°C. Figure 11 shows that even after 90 minutes at 800 rpm the slags were far from saturation, reflecting the high slag mass to sample ratio and the relatively slow kinetics of the dissolution process.

The results presented in Figure 11 indicate that for Slag 1 the rate of degradation in the first 15 minutes increased with rotation speed up to about 600 rpm after which the rate reached a maximum (decreased slightly). This suggests that it is likely that the reaction is controlled by mass transfer at speeds up to about 600 rpm, when chemical reaction rate becomes dominant. However, for Slag 2 the rate of degradation in the first 15 minutes continued to increase with rotation speed above 600 rpm. This indicates that flow rates, which result in chemical reaction rate control being dominate, have not been reached for this system.

The results for Slag 1 (no Al_2O_3) at 800 rpm shown in Figure 12 suggest that the rate of degradation is approximately proportional with time (approx. 0.1 wt% MgO/minute) and that lowering the temperature to 1500°C has very little effect on the reaction rate. Microstructural examination showed that intergranular penetration was restricted to a narrow surface region approximately 20 to 100 μm in width. Three phases were present in the solidified slag: pseudowollastonite ($CaO.SiO_2$), rankinite ($3CaO.SiO_2$) and glass. None of these would be expected to be solid at the test temperature, and would form when the sample was cooled. In this slag the MgO undergoes congruent dissolution.

The results for Slag 2 (20% Al_2O_3) at 1530°C and 800 rpm suggest that the rate of degradation is approximately proportional with time (approx. 0.1 wt% MgO/minute), which is consistent with the results obtained for Slag 1. However, lowering the temperature to 1500°C did have a significant effect on the reaction rate, almost halving the rate of MgO pick-up in the slag.

Discussion

These results show two distinctly different modes of MgO degradation occurring at the extremes of the experimental conditions. In low flow rate experiments the degradation is dominated by the dissolution of MgO at the slag/refractory/air interface where highly localized fluid flows are created by the interfacial tension gradients established as the MgO dissolves into the slag. This form of degradation is almost certainly mass transfer controlled; that is, the rate of dissolution is governed by the rate of mass transfer of dissolved MgO in slag in the region close to the slag/refractory/air interface. In contrast, the experiments at 800 rpm it is clear that degradation is dominated by degradation near the base of the submerged sample. The characteristic 'coning' of the samples indicates that there is accelerated degradation of refractory from the weakest mechanical point of the sample as it is spinning. It was observed that some MgO grains had been detached from the sample and were reacting with the slag. This means that the erosion/corrosion profile formed, in part, reflects the mechanical aspects of how a spinning cylinder interacts with a fluid.

Supplied by Rojan Advanced Ceramics, Henderson, Western Australia

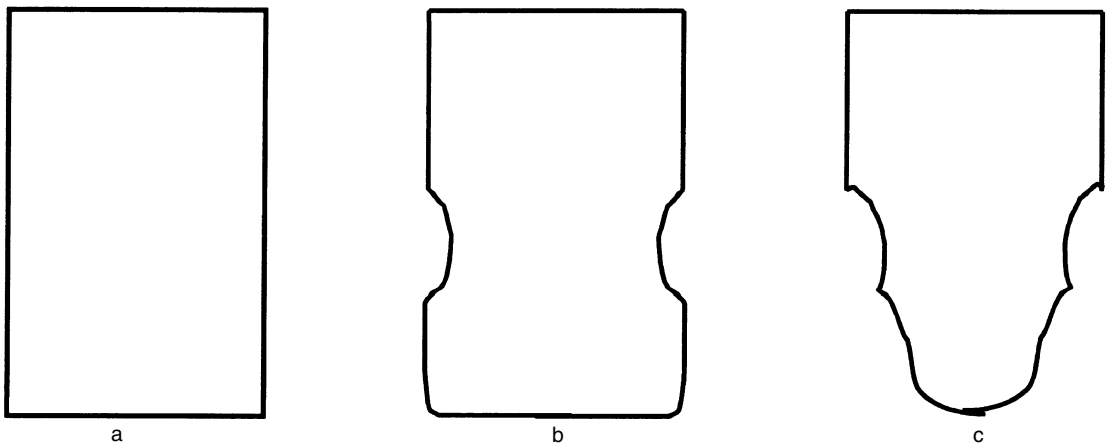

Figure 10. Profile of MgO samples (a) original profile, (b) after testing at high speed for short time, (c) after testing at high speed for a longer time

Table VI
MgO content of slag at completion of experiment (mass %)

Slag 1 46% SiO_2 46% CaO 5% FeO_x 3% MgO						Slag 2 36% SiO_2 36% CaO 20% Al_2O 35% FeO_x 3% MgO					
T= 1530°C											
Speed (rpm)	15 min	30 min	45 min	60 min	90 min	Speed (rpm)	15 min	30 min	45 min	60 min	90 min
50	3.9					50	3.5				
200	4.7					200	4.3				
400	5.3					400	4.7				
600	5.7					600	5.5				
800	5.3	6.7	10.4	10.6	12.6	800	5.8	7.0	8.6	9.9	11.8
T=1500°C											
Speed (rpm)						Speed (rpm)					
600	5.8					600	4.4				
800	5.7		9.3		13.0	800	3.7	5.6		5.9	8.3

In the case of the experiments without alumina in the slag, the independence of dissolution rate from speed above 600 rpm supports the notion that the rate of dissolution at 800 rpm is chemically controlled (i.e. not mass transfer), though this is not the case for experiments involving alumina where the rate is still increasing with increasing rotation speed. What is most interesting about experiments at 1530°C and 800 rpm for slags with alumina is that the overall rate is very similar to slags without alumina, indicating that any spinel formed is not providing significant protection to degradation of MgO refractories .

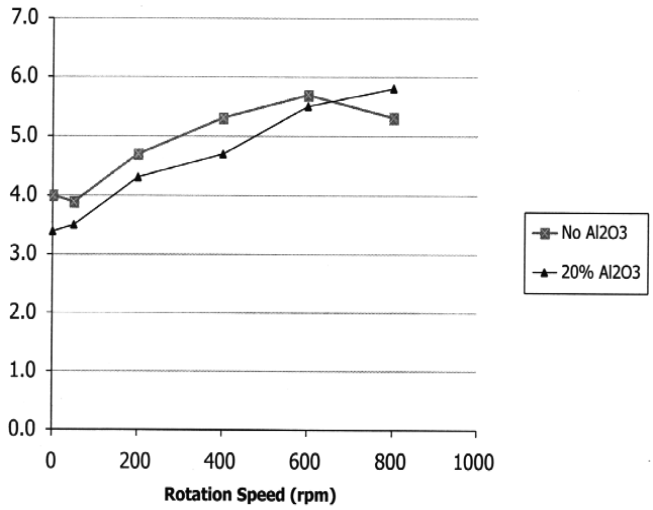

Figure 11. MgO content of the slag after 15min test at 1530°C as a function of rotation speed

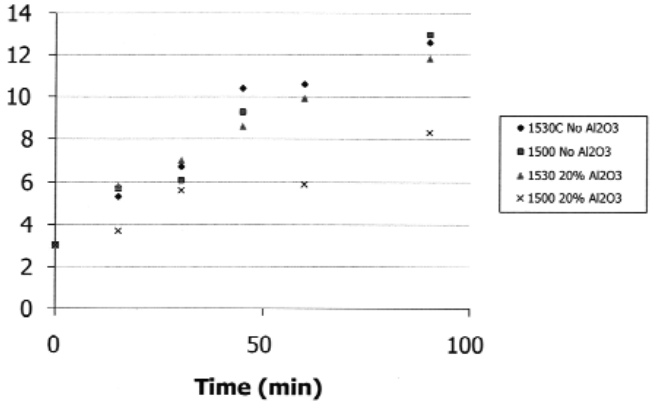

Figure 12. MgO content of the slag after testing at 800 rpm as a function of time

The differing effects of temperature on the dissolution rate of the samples in alumina containing slags compared to non-alumina slag is also very interesting. In the case of slags with alumina, the overall dissolution rate is halved by lowering temperature from only 1530 to 1500°C (as can be seen in Figure 12), indicating that the overall rate is strongly influenced by spinel formation. Micrographs show that a greater number of smaller spinel grains formed at the lower temperature, and that they formed a more coherent layer than at 1530°C, as shown in Figure 13. At 1530°C, the spinel forms as discrete grains separated from the MgO interface, or connected at asperities forming small 'bridges' and providing little protection from further dissolution. This morphology is in agreement with the model described by Sandhage *et al.* in their work on alumina dissolution in $CaO-MgO-Al_2O_3-MgO$ melts[4]. At 1500°C most of the spinel was still separated from the MgO by a slag layer, but there was greater cohesion of the spinel layer. This would provide a more effective barrier to dissolution.

Incongruent dissolution has resulted in a more complex mechanism in which the formation of a reaction product can retard dissolution if the temperature is low enough to cause nucleation and growth of a coherent product layer. It must be noted that after 90 min at 1500°C and 800 rpm this layer appeared to have been partially removed, with those spinel grains attached at asperities or trapped in surface pores remaining at the solid/liquid interface. Other spinel grains appeared to have become detached and washed out into the slag.

Formation of a spinel layer on parts of the magnesia sample furnace give rise to a complex corrosion mechanism in which diffusion of reactants through the spinel layer is necessary for further corrosion of the magnesia to occur. This would be expected to slow the overall dissolution rate.

Conclusions

The LSCM technique is capable of measuring dissolution phenomena in transparent slag systems, though rate data measured using this technique are subject to as yet unquantified uncertainty. This uncertainty is at least in part due to the fact that certain phenomena are being observed for the first time. Developing a better understanding of the

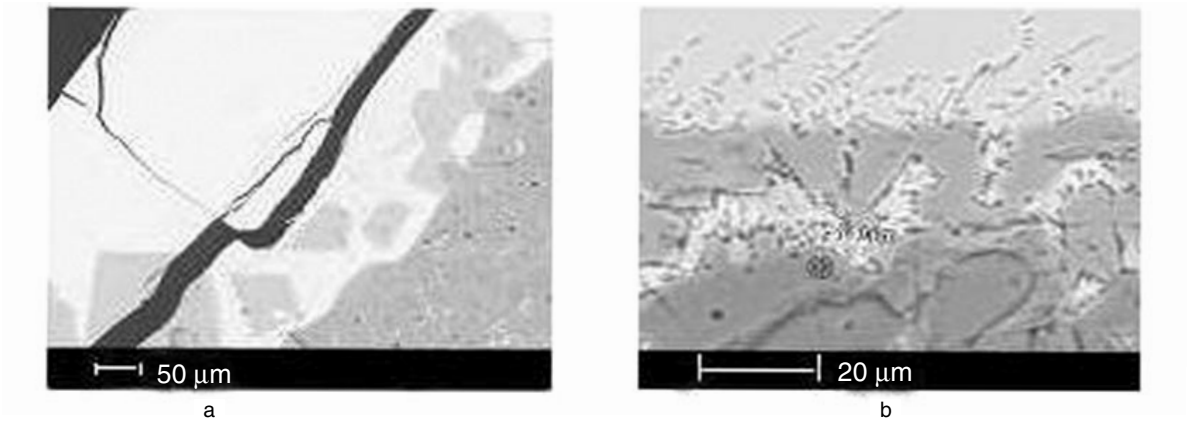

Figure 13. Spinel formation after 15 minutes at (a) 1530°C and (b) at 1500°C, 800 rpm

phenomena observed in the LSCM is likely to be the focus of much future research.

The dissolution of alumina micro-particles in slags of compositions used in this study was found to be controlled by mass transfer in the slag.

The values of the diffusion coefficients for alumina particles in $CaO-SiO_2-Al_2O_3$ slags used in this study were in reasonable agreement with other reported data and ranged from 10^{-11} to 10^{-10} m^2s^{-1} over a temperature range of 1477 to 1577°C.

Studies of congruent dissolution of MgO in $CaO-MgO-Al_2O_3-SiO_2-FeO_x$ slag using rotating finger tests show that dissolution is controlled by mass transfer at speeds up to about 600 rpm, beyond which chemical reaction rate appears to become dominant. Addition of Al_2O_3 to the slag resulted in the formation of some spinel at the interface, complicating the dissolution mechanism. This did not reduce the rate of dissolution of the MgO at the higher test temperature, but significantly reduced the rate when the temperature was reduced to 1500°C.

These experiments show that formation of a solid reaction product at the interface does not necessarily reduce dissolution rates of the refractory. The morphology and distribution of the product, and its ability to withstand mechanical forces imposed by flowing liquids, must also be taken into consideration.

References

1. LEE, W.E. and ZHANG, S. Melt corrosion of oxide and oxide-carbon refractories, *International Materials Reviews,* vol. 44, 1999, pp. 77–104.
2. SANDHAGE, K. and YUREK, G. Direct and indirect dissolution of sapphire in calcia-magnesia-alumina-silica melts, *Journal of the American Ceramic Society,* vol. 73, 1990, pp. 3633–3342.
3. SANDHAGE, K. and YUREK, G. Indirect dissolution of sapphire in calcia-magnesia-alumina-silica melts, *Journal of the American Ceramic Society*, vol. 73, 1990, pp. 3643–3649.
4. SANDHAGE, K. and YUREK, G. Indirect dissolution of sapphire into silicate melts, *Journal of the American Ceramic Society*, vol. 71, 1988, pp. 478–489.
5. TAIRA, S., NAKASHIMA, K., and MORI, K. Kinetic behaviour of dissolution of sintered alumina into $CaO-SiO_2-Al_2O_3$ slags, *ISIJ Int*., vol. 33, 1993, pp. 116–123.
6. TAIRA, S., MACHIDA, A., NAKASHIMA K., and MORI, K. Effect of MgO on the dissolution rate of Al_2O_3 in molten $CaO-SiO_2-Al_2O_3-MgO$ slags, *Journal of the Iron and Steel Institute of Japan*, vol. 82, 1996, pp. 1–5.
7. UEDA, K. Dissolution rate of Al_2O_3 in molten $CaO-SiO_2-Al_2O3$ slags, *Journal of Japan Institute of Metals*, vol. 63, 1999, pp. 989–993.
8. YU, X., POMFRET R.J., and COLEY, K.S. Dissolution behaviour in mould fluxes, *Metallurgical and Materials Transactions B*, vol. 28B, 1997, pp. 275–279.
9. COOPER, A.R. and KINGERY, W.D. Dissolution in ceramic systems, J*ournal of the American Ceramic Society*, vol. 47, 1964, pp. 37–43.
10. SRIDHAR, S. and CRAMB, A.W. Kinetics of dissolution in $CaO-MgO-SiO_2-Al_2O_3$ slags. *Metallurgical and Materials Transactions B*, vol. 31B, 2000, pp. 406–410.
11. VALDEZ, M., PRAPAKORN, K., CRAMB, A.W., and SRIDHAR, S. A study of the dissolution of Al_2O_3, MgO and $MgAl_2O_4$ particles in a $CaO-SiO_2-Al_2O_3$ slag, *Steel Research*, vol. 72, 2001, pp. 291–297.
12. LEE, S.H., TSE, C., YI, K.W., MISRA, P., CHEVRIER, V., ORRLING, C., SRIDHAR, S., and CRAMB, A.W. Separation and Dissolution of Al_2O_3 inclusions at slag/metal interfaces. *Journal of Non-Crystalline Solids*, 282, 2001, pp. 41–48.
13. PHELAN, D.J. and DIPPENAAR, R.J. *In situ* study of the early stages of solidification. *The Brimacombe Memorial Symposium*. Irons G.A. and Cramb A.W. (eds.), Vancouver, Canada, TMS, 2000, pp. 579–593.
14. CHOI, J.Y., LEE, H.G., and KIM, J.S. Dissolution rate of Al_2O_3 into molten $CaO-SiO_2-Al_2O_3$ slags, *ISIJ Int*., vol. 42, 2002, pp. 852–860.
15. CHO, W.D. and FAN, P. Dissolution behaviour of alumina particles in molten slags, *EPD Congress and Fundamentals of Advanced Materials for Energy Conversion*, Taylor, R. (eds.), TMS, USA, 2002, pp. 631–638.
16. LEVENSPIEL, O. *The Chemical Reactor Omnibook*, OSU Book Stores Inc., Oregon, USA, 1989, pp. 51.1–51.6.
17. POIRIER, D.R. and GEIGER, G.H. *Transport Phenomena in Materials* Processing, TMS, Warrendale, PA, USA, 1994, pp. 444-453.

18. DAVIES, R.H., DINSDALE, A.T., GISBY, J.A., HODSON, S.M., and BALL R.G.J. Thermodynamic modelling using MTDATA, *Proc. Conf. Applications Thermodynamics on the Synthesis and Processing of Materials*, ASM/TMS, Rosemont, IL, USA, 1994, pp. 371–384.

19. MILLS, K.C. *Slags Model version* 1.07, National Physical Laboratory, London UK, 1986.

20. TOULOUKIAN, Y.S., KIRBY, R.K., TAYLOR R.E., and LEE T.Y.R. *Thermophysical Properties of Matter*, vol. 13, IFI/Plenium, New York, 1977, pp. 176–176.

21. HENDERSON, J., YANG, L., and DERGE, G. *Trans. Metall. Soc*., vol. 211, 1961, p. 56.

22. *Slag Atlas*, 2nd Edition, Mills, K.K. (eds.), Verlag Stalheisen GmBH, Dusseldorf, Germany, 1995, pp. 349–353.

23. BYGDEN, J., DEBROY T., and SEETHARAMAN, S. Dissolution of MgO in stagnant CaO-FeO-SiO_2 slags, *Ironmaking and Steelmaking*, vol. 21, 1994, pp. 318–323.

24. ALLEN, N., SUN, S., and JAHANSHAHI, S. Stability of MgO refractory in contact with iron-rich slags, *2nd Melt Chemistry Symposium*, Melbourne, Australia, 1995, pp. 55–59.

25. ZHANG, P. and SEETHARAMAN, S. Dissolution of MgO in CaO-'FeO'-CaF_2-SiO_2 slags under static conditions, *J. Am. Ceram. Soc*., vol. 77,1994, pp. 970–976.

26. WALLACE, M., SUN, S., and JAHANSHAHI, S. Thermodynamic constraints on slag-refractory interaction: the effect of oxygen potential on spinel and wustite stability in the MgO-FeO-Fe_2O_3 system, *6th AusIMM Extractive Metallurgy Conference*, Brisbane, Australia, 1994, pp. 37–40.

27. VADASZ, P. and MOLNAR, L. Interaction at the periclase-slag melt phase boundary, *Ceramics-Silikaty*, vol. 36, 1992, pp. 199–204.

28. GOTO, K., ARGENT B.B., and LEE, W.E. Corrosion of MgO-$MgAl_2O_4$ spinel refractory bricks by calcium-aluminosiicate slag, *J. Am. Ceram. Soc*., vol. 80, 1997, pp. 461–471.

29. RAIT, R. PhD thesis, University of Melbourne, Australia, 1997.

30. TRAN, T., NIGHTINGALE, S., and BROOKS, G. Corrosion of MgO by alumina containing slags, *J. Aust. Ceram. Soc*., vol. 34, 1998, pp. 33–38.

31. DUNKL, M. and BRUCKNER, R. Corrosion of refractory materials by a container glass melt under the influence of various convection flows, *Glastech Ber*, vol. 60, 1987, pp. 261–267.